TECHNICAL ARTICLE

A 2D pixel detector for very high-rate X- and gamma-ray spectroscopy and imaging

Einar Nygård,[1,a)] Nail Malakhov,[1] Peter Weilhammer,[1,2,†] Ole Dorholt,[3] Ole M. Røhne,[3] Terumasa Nagano,[4] and Koei Yamamoto[4]
[1]*Enxense AS, Asker, Norway*
[2]*CERN, Geneva, Switzerland*
[3]*University of Oslo, Norway*
[4]*Hamamatsu Photonics, Hamamatsu City, Japan*

(Received 16 March 2017; accepted 26 March 2017)

A new methodology for very high-speed, energy-dispersive detection of X-ray fluorescence is being developed. The underlying reasoning behind it, as well as early results from the evaluation of the first prototype, is presented. © *2017 International Centre for Diffraction Data.*
[doi:10.1017/S0885715617000392]

Key words: detector, XRF, ED-XRF, micro-XRF, XRD, hybrid-pixel, high-rate, high-spectral-resolution

I. INTRODUCTION

A two-dimensional (2D) pixel detector concept with full spectroscopy feature in each pixel has been developed. The concept is versatile and can be applicable for a variety of uses, but is initially targeted for very high-rate energy-dispersive X-ray fluorescence (EDXRF). The concept, named HPXD, allows for extremely high rate capacity per mm^2, upholding of the rate capacity per mm^2 independent of detection area, and upholding of the energy-resolution independent of detection area. Furthermore, it is suitable for being used with sensor material made of Silicon or Cd(Zn)Te. It also has the capability of providing full-field XRF imaging, and, it allows for construction of monolithic large surface detectors. Used and tested as an EDXRF detector, the first prototype has a conceptual input rate capacity of $\sim 10^7$ photons s^{-1} mm^{-2}, and a measured energy resolution of 250 eV.

II. BACKGROUND

Today's EDXRF detectors are based mostly on Silicon-Drift Detectors (SDDs). The principle of the SDD is that it yields high area-coverage on its cathode (that is facing the X-rays), whereas through the drift-structure the anode is tiny to yield the very best low-noise qualities (Lechner *et al.*, 2004). However, despite this ingenious concept, it does not exploit the highest rate-capability potential of a silicon detector, since there is just one single signal output channel for the entire detector, as illustrated in Figure 1. The rate capacity of this single output channel is a limiting factor of a SDD's total rate capacity. This limited output rate capacity is fairly constant regardless of the SDD's detection area, and therefore, the saturation rate/mm^2 of the SDD will drop off inversely proportional to its detection surface area (see Figure 2). Quite large surface area SDDs exist today (150 mm^2 is reported), made for the purpose of covering the largest possible solid angle in an XRF measurement.

However, if a detector is already close to rate saturation for a given solid angle, the SDD's detection area cannot simply be increased to increase the overall measurement speed. Because of the larger area, and thereby proportionally more impinging photons, would simply cause oversaturation of the output channel.

III. 2D PIXEL ARCHITECTURE

The 2D pixel detector, or hybrid pixel detector, for detection of particles, X-, and gamma-rays is a well-known method that has been in use for various applications for more than a decade (Wermes, 2004; Rossi *et al.*, 2006). The physical principle is depicted in Figure 3. In this principle, the top-layer (that is facing the radiation) is a matrix of sensor elements (pixels) that is formed in one single semiconductor crystal piece. The sensor elements will convert X-rays that impinge within a pixel's boundary, into an electric charge. This conversion process is similar to that of the SDD, except the

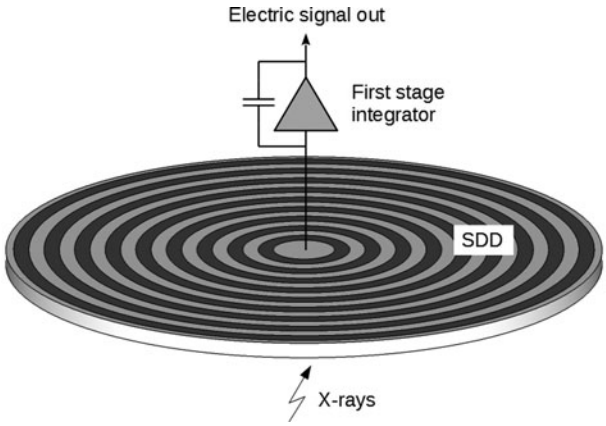

Figure 1. SDD and its output channel.

[a)]Author to whom correspondence should be addressed. Electronic mail: einar@enxense.com
† In memory of the great Peter Weilhammer (1938–2016), friend, mentor and contributor to this project.

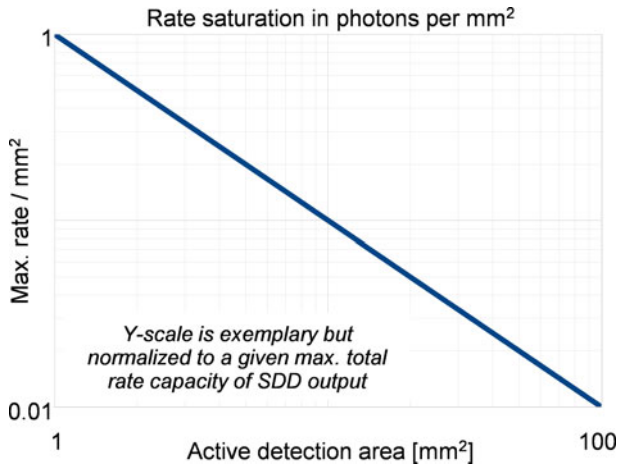

Figure 2. (Colour online) Saturation rate/mm^2 of SDDs.

pixel sensor elements are more PIN type diodes than they are drift-type diodes (Beckhoff *et al*., 2007). The charge signal generated in a pixel, as a response to an X-ray, is transferred to the bottom layer of the sandwich via a small electrically conductive ball that is connected to the anode of each pixel. These balls are commonly referred to as bumps and the process of doing it is called bump-bonding or flip-chip assembly. The bottom layer is an integrated circuit, IC, typically in CMOS technology. This Application Specific IC, ASIC, is arranged in a pixel structure too, with a physical layout identical to the pixel structure of the sensor layer on top. All the pixels in the ASIC are identical in function, and the first

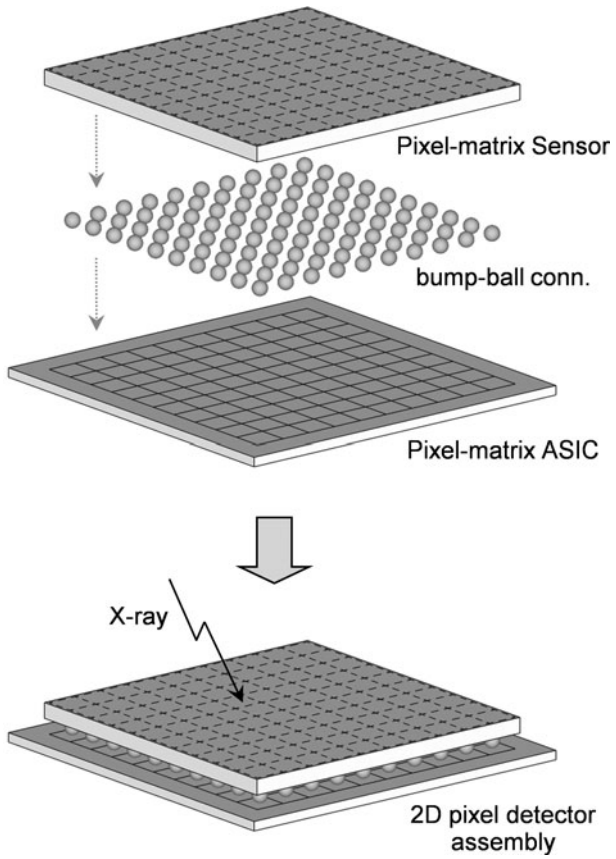

Figure 3. 2D pixel architecture.

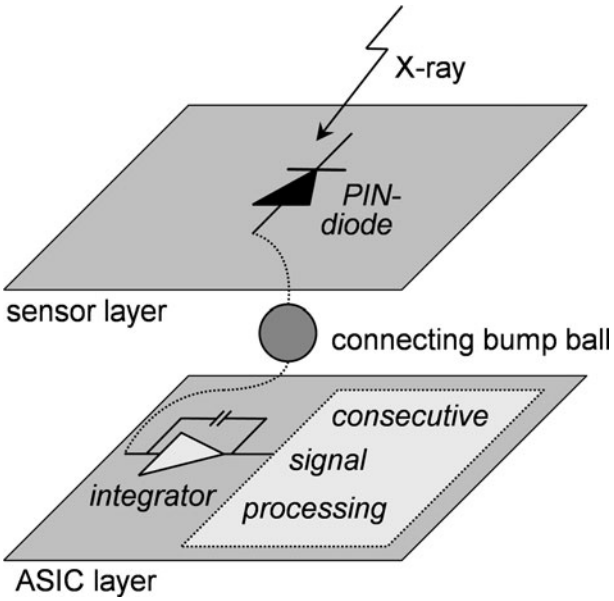

Figure 4. In each pixel.

circuitry in them is a first stage integrator, similar to the integrator stage of the SDD (Figure 1). Following this integrator, there is usually more consecutive signal processing in each of these ASIC pixels, as indicated in Figure 4. Generally, in most 2D pixel detectors, the functional structure is like this.

IV. OUR HPXD/2D PIXEL DEVICE FOR EDXRF

The generic principle of 2D pixel detectors is well suited also for detection of fluorescent X-rays. As explained before, in applying this principle a much higher count rate capacity per mm^2 can be obtained when comparing with the common SDD principle. This is because the sensor now includes a multiple of sensor elements, and an equal multiple of output channels, that individually can operate fully in parallel. The higher rate capacity will be achieved if the individual spectrum of all the pixels is superimposed into one summed spectrum. In using this 2D pixel concept in EDXRF, the rate capacity per mm^2 will be independent of detection area and only be limited to the maximum rate of one pixel divided by the surface area (pixel size) of that single pixel. In the current first prototype presented here, the conceptual maximum rate of one pixel is about 500 kcps, and the pixel size is 250 μm × 250 μm = 1/16 mm^2 making the saturation rate about 8 Mcps mm^{-2}. (Related to available baseline-restore feature, the estimated total dead-time per count in the amplifier/trigger is 2 times the peaking time [about one 1 μs in this case]. Based on this, conventional Poisson count-loss analysis is applied to yield the 500 kcps maximum rate estimate.) This rate is possible to maintain over the entire detector surface, regardless of its total area (Figure 5). There is naturally a data-acquisition (DAQ) side to this, and therefore, the larger the area, the more powerful the DAQ needs to be if one wants to uphold this maximum rate over a very large detector surface. This is however manageable through fairly standard electronics. The structure of our HPXD also has some other advantages when comparing with the SDD. One is that both the silicon pixel sensor, and the ASIC, is simple to scale and devices larger than the present largest SDDs currently on the market can relatively

https://doi.org/10.1017/S0885715617000392 Published online by Cambridge University Press

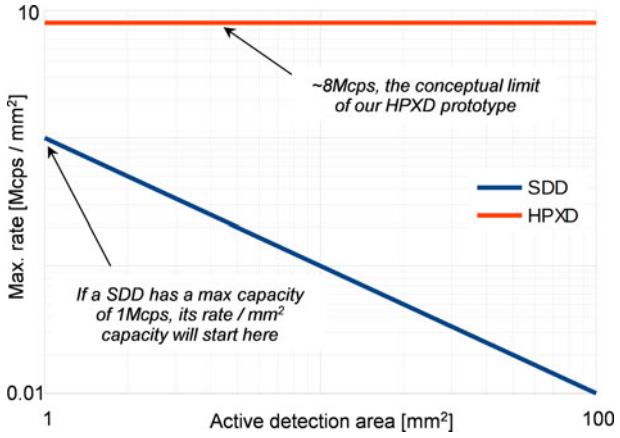

Figure 5. (Colour online) Rate per mm^2 comparison our HPXD vs. a 1 Mcps SDD.

straight forwardly be made. Another advantage is that the silicon pixel detector can more easily be made considerably thicker than the commonly used thickness of today's SDDs (450 μm), something which significantly improves detection efficiency at the higher X-ray energies (Schlosser *et al*., 2010). In addition, the HPXD structure allows for more easy utilizing of Cd(Zn)Te [Cadmium (Zinc) Telluride] as the sensor material to allow for even better detection efficiency at the higher X-ray energies (see more about this in Section VII).

V. HOW OUR HPXD WORKS

In addition to the functions of the PIN-diode and the first stage integrator (Figure 4), there is a fair amount of consecutive signal processing in each ASIC pixel in order to handle the signal as needed for spectroscopy. There also will be signal post-processing in a downstream DAQ system, external to the HPXD detector, but the HPXD pixels need an appropriate amount of pre-processing done in order to send the spectroscopic data to that downstream DAQ. This is done on a per-pixel basis and a flowchart of this is shown in Figure 6. With reference to the numbering of the flowchart elements, the functionality is as follows: (1) the X-ray impacts; (2) the sensor PIN-diode converts the X-ray energy to a proportional amount of electric charge; (3) the charge gets integrated (in the first stage integrator), amplified and shaped to a semi-Gaussian voltage pulse, after which the signal is split in two branches; (4) the semi-Gaussian peak-level gets stretched in time (this stretched peak-level is proportional to the X-ray energy); (5) a discriminator checks if the signal is above a preset threshold; (6) creation of a sample/hold signal after some delay; (7) a S/H unit dynamically holds the stretched peak-level; (8) a one-digit analogue "ROM" stores the pixel address as an analogue signal level; (9) function that checks if the data-bus is free; (10) function that reserves the data-bus; (11) creation of a signal that enables the analogue output ports; (12) analogue output ports for the stretched peak-level as well as for the analogue pixel address; (13) output of the data to data-bus (an analogue data-bus, which is common to a multiple of pixels and which leads to the downstream DAQ); (14) creation of a reset-all signal following a preset delay; (15) reset all.

For each impinging X-ray with an energy that produces an amplified signal higher than the preset level in the discriminator, the explained signal processing will result in the generation of two analogue "data-packages" as indicated in Figure 7. These data-packages are two analogue levels that appear on the data-bus for a short duration. The values (analogue levels) of the two data-packages represent the X-ray energy, and the pixel address, respectively. Even if, in fast operation, the X-ray energies from all pixels will be superimposed into one summed spectrum, pixel address information is needed so that each pixel can be perfectly calibrated using the gain- and offset-variations, which inevitably will exist between pixels. Returning to Figure 6, the functions 9 and 10 represent a hand-shake mechanism that serves as a "traffic-control". This is to avoid collisions on the data-bus between two or more pixels that may want to access the data-bus at similar times, due to the random nature of the X-ray incidents. This function also includes an arbitration mechanism that allows for a buffer queue of pixels that are denied immediate access to the data-bus. This traffic-control allows for minimal data-loss in the detector.

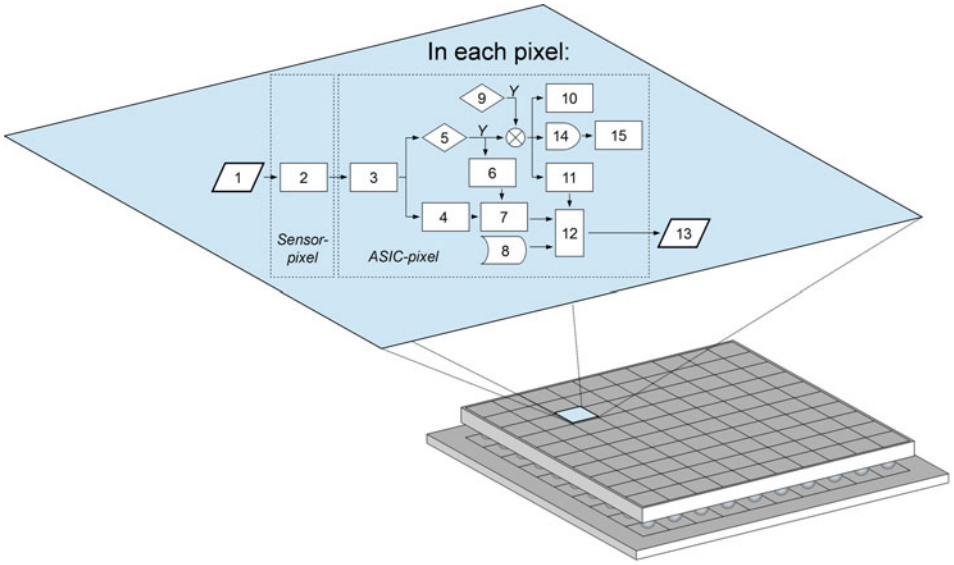

Figure 6. (Colour online) In-pixel functionality.

https://doi.org/10.1017/S0885715617000392 Published online by Cambridge University Press

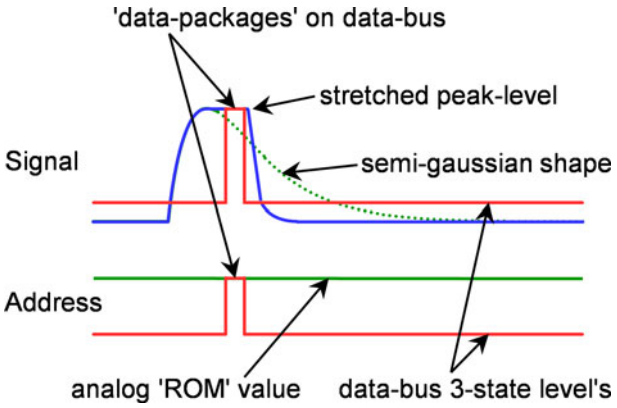

Figure 7. (Colour online) Signals-to-output creation.

As explained, each pixel in the HPXD detector is sufficiently self-contained to automatically handle each X-ray that is incident within its boundaries. For each event a given pixel detects, it will "push" the corresponding data-packet to the downstream DAQ in an automated data-driven fashion (as depicted in Figure 8). This data-packet transfer can be significantly faster than the average time between pixel-events, so the data-transfer bus can be shared between many pixels. Depending on the chosen configuration, the system will typically also use parallel data-transfer buses. In the current prototype of 10×10 pixels, groups of 10 pixels share one bus and there are consequently 10 parallel buses.

VI. RESULTS

A first prototype has been successfully developed and tested. The photo in Figure 9 shows the 2D pixel-matrix CMOS ASIC assembled on a PCB for testing. As explained, the matrix consists of a total of 100 pixels in a 10×10 arrangement. Each pixel is $250\ \mu m \times 250\ \mu m$, and the entire active matrix is thus 2.5 mm × 2.5 mm. Power and all the IO terminals, including the data-buses, can be seen connected to the PCB by bond-wires. The photograph in Figure 10 also shows the ASIC and the PCB, but here the 2D pixel-matrix Silicon sensor is also shown. The active PIN-diode pixel elements of this sensor, as well as the 2D matrix arrangement, have the same exact geometries as of the ASIC, i.e., 100 pixels, 10×10 matrix, $250\ \mu m \times 250\ \mu m$ pixel-size and 2.5 mm × 2.5 mm total active area, making the detection surface 6.25 mm^2. The sensor can be seen precisely aligned on top

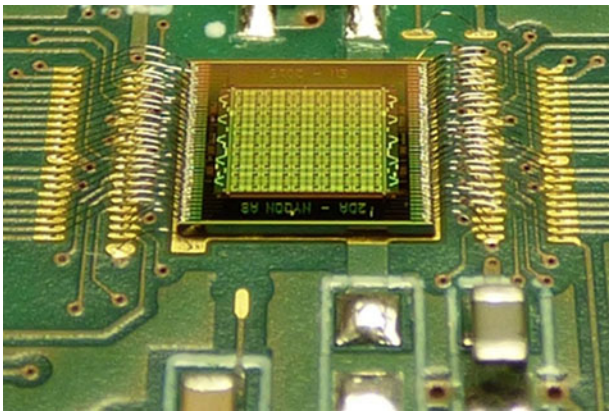

Figure 9. (Colour online) Pixel ASIC on test PCB.

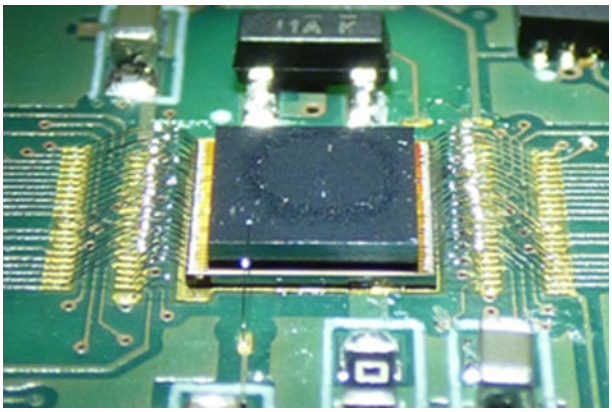

Figure 10. (Colour online) Pixel sensor mounted on the ASIC.

of the ASIC. The 100 total pixels in the ASIC and the sensor, respectively, are connected to each other by bump-balls, even though not visible in this photo. This ASIC/bump-balls/sensor module constitutes the HPXD detector.

In tests, our prototype HPXD shown in the previous photos, exhibits full functionality to specifications. The ASIC, which comprises the biggest variety of features, was designed to be quite versatile, also for detailed function-testing purposes. In test mode, it is possible to probe into each pixel and study signal responses at different stages in the signal processing explained in the flowchart diagram (Figure 6). Shown in Figure 11, below, is an oscilloscope trace of the output of flowchart element 3, the semi-Gaussian shaper output, as a

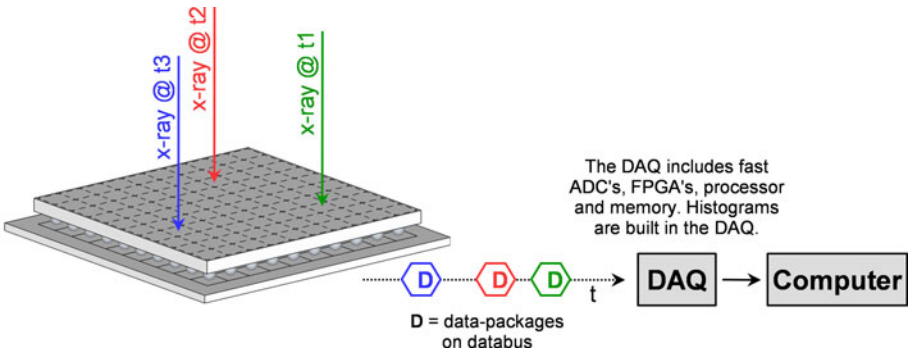

Figure 8. (Colour online) Transfer of data-packages.

https://doi.org/10.1017/S0885715617000392 Published online by Cambridge University Press

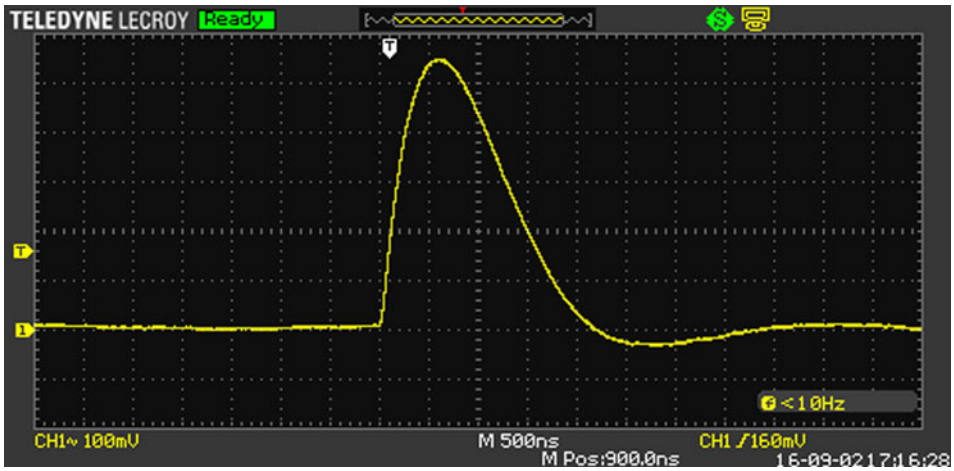

Figure 11. (Colour online) Output of semi-Gaussian shaper.

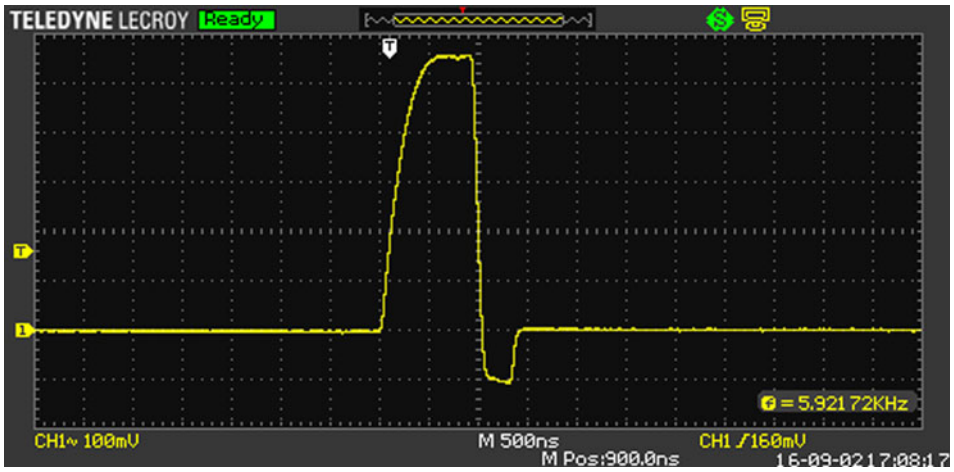

Figure 12. (Colour online) Output of stretcher.

response to an incident X-ray. Figure 12 shows the output of flowchart element 4, the stretched peak of the semi-Gaussian shape, as a response to another incident X-ray (the shaper is approximately a first order CR-RC type for which integration time equals peaking time, here 500 ns). In the latter example, also the discriminator is enabled and therefore the pixel being reset and reactivated is also visible (following the stretched peak period).

Our HPXD has been tested with an industrial type ^{55}Fe radioisotope (1 GBq) that produces X-rays predominantly at 5.9 keV (25.4%) and 6.5 keV (3%). When initializing the ASIC for normal operation and placing this source above the sensor, the data-driven functionality immediately makes the device respond with a stream of data-packages on the data-buses. Figure 13 is an oscilloscope snapshot showing this.

The upper trace displays a stream of the X-ray energy data-packages, whereas the lower trace is the corresponding stream of the address data-packages. That is, for each X-ray's data-package there is an energy value and a corresponding address value carrying information about in which pixel the X-ray was captured. Both traces are in the form of short-duration analogue voltage-level pulses. The exemplary, but real, data-package stream shown here represents far from the maximum rate that can be obtained.

The 10 parallel data-package streams (data-buses) in the present prototype are received by our DAQ system which is digitizing the data-package's voltage levels by ADC conversion. Based on the pixel-address value, the energy value is sorted and added to a histogram (spectrum) memory reserved for that pixel only. Consequently, 100 individual spectra are initially created. After calibration of each spectrum individually, these spectra can be used as they are if the HPXD is used for full-field EDXRF imaging, in which case the rate per pixel would be ordinarily fast. However, in the case of being used as a faster alternative to single-channel SDDs, the individual spectra must be superimposed into one summed spectrum. If the calibration per pixel's spectrum is precise, there will be next to a negligible penalty in the summed spectrum quality when performing such summing.

The spectra in Figures 14 and 15 were acquired by our HPXD at a sensor temperature of about −10 °C. One spectrum is taken from just one single pixel, whereas the other spectrum is the sum of 30 pixels, and confirms that the spectrum quality remains the same after the summing (~250 eV energy resolution in both cases). Signal integration time for all pixels is 500 ns. There are a couple of mentionable issues with these spectra that relate to the fact that these are very early stage results; One is the difference in shape between the two

https://doi.org/10.1017/S0885715617000392 Published online by Cambridge University Press

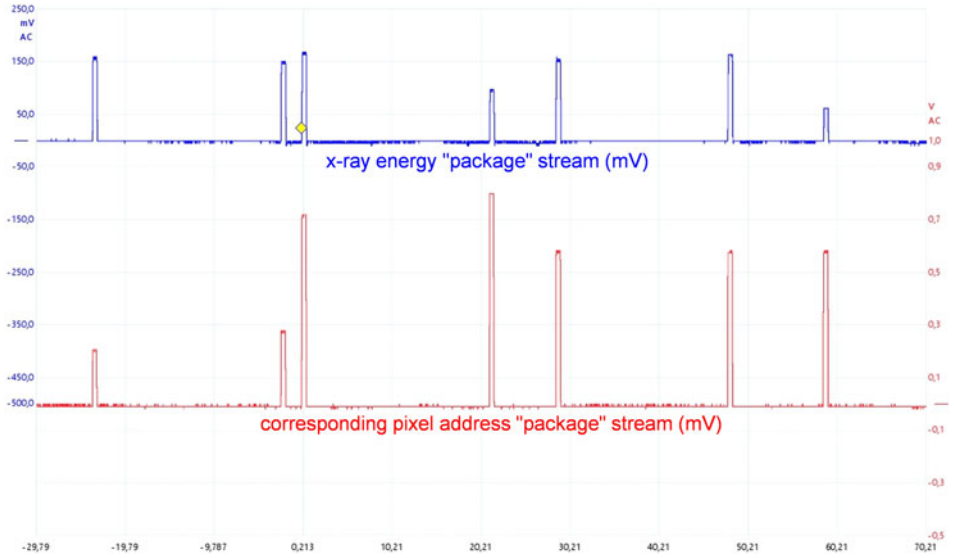

Figure 13. (Colour online) Data-package stream.

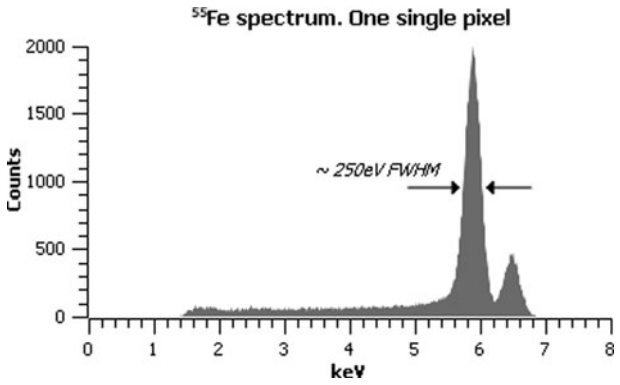

Figure 14. Single pixel spectrum.

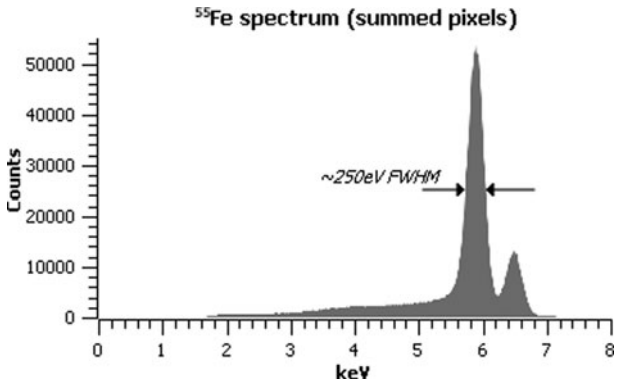

Figure 15. Spectrum of 30 pixels summed.

spectra below 3.5 keV, which is a result of some pixels having a different threshold than other pixels, and, the other is that only 30 pixels are included in the summed spectrum, because the DAQ was not fully completed at the time of these measurements. The quite early results reported here are very satisfying for this first version device, and are quite in line with our initial ambitions.

VII. NOTES

Even though the rate capability of our HPXD is superior, the demonstrated energy resolution of 250 eV (@ 5.9 keV) is not quite on par with today's state-of-the-art SDD devices. Keep in mind, however, that the excellent energy resolution reported for the present state-of-the-art SDDs is always measured at 5.9 keV, and that the Fano-corrected statistical fluctuation in any silicon sensor defines a limit to the SDD performance (Beckhoff *et al*., 2007). At 20 keV, for instance, the energy resolution of a SDD cannot be better than 210 eV for this reason, also for SDDs. The energy resolution specifications given therefore represent a simplified truth, because they are measured at 5.9 keV and not at higher energies.

There is also improvement potential in our HPXD technology and achieving an energy resolution of 150 eV (@ 5.9 keV) in the future is within reach. Also, the concept of the HPXD of summing spectra from many small pixels will have a particular benefit if applying sensor types other than silicon, for instance Cd(Zn)Te material. This is because such sensor material is not easily arranged in the special SDD geometry (Figure 1) and small area pixels are therefore essential to obtain the best energy resolution. The high stopping power of such Cd(Zn)Te material, easily stopping X-rays up to 100 keV, makes it particularly suited in XRF on K lines of rare earth metals, lead, gold, uranium, and other high *Z* materials. We expect to pursue a branch in our future activity to such sensor material, with the ambitions of obtaining 300 eV energy resolution or better.

VIII. CONCLUSIONS

This development has progressed very successfully, and we have demonstrated a successful development of a new breed of EDXRF sensors that has superior count rate capability to the conventional SDD. We have also demonstrated an energy resolution close to our own initial target for this first prototype. Furthermore, we see a realistic path forward to make the energy resolution come close to the resolution of state-of-the-art SDDs, and, we see a clear path forward to a product for high-*Z* XRF, which can be superior to existing detectors, for sure in count rate capability, but also in energy-resolution.

https://doi.org/10.1017/S0885715617000392 Published online by Cambridge University Press

ACKNOWLEDGEMENTS

We acknowledge the Norwegian Research Council for their support, and partial funding, of the R&D in this project. Thanks also to Hamamatsu Photonics for their corporate support of this project as well as their contribution of the silicon sensor used, and bump-bonding, and, to the Physics Department of the University of Oslo for their contribution in doing R&D on bump-bonding technology.

Beckhoff, B., Kanngießer, B., Langhoff, N., Wedell, R., and Wolff, H. (**2007**). *Handbook of Practical X-Ray Fluorescence Analysis* (Springer Science & Business Media, Berlin).

Lechner, P., Fiorini, C., Longoni, A., Lutz, G., Pahlke, A., Soltau, H., and Strüder, L. (**2004**). "Silicon drift detectors for high resolution, high count rate x-ray spectroscopy at room temperature," International Centre for Diffraction Data 2004, Advances in X-Ray Analysis **47**, 53–58.

Rossi, L., Fischer, P., Rohe, T., and Wermes, N. (**2006**). *Pixel Detectors: from Fundamentals to Applications* (Springer Science & Business Media, Berlin).

Schlosser, D. M., Lechner, P., Lutz, G., Niculae, A., Soltau, H., Strüder, L., Eckhardt, R., Hermenau, K., Schaller, G., Schopper, F., Jaritschin, O., Liebel, A., Simsek, A., Fiorini, C., and Longoni, A. (**2010**). "Expanding the detection efficiency of silicon drift detectors," Nucl. Instrum. Methods Phys. Res. A **624**, 270–276.

Wermes, N. (**2004**). "Trends in pixel detectors: tracking and imaging," IEEE Trans. Nucl. Sci. **51**, 1006–1015.